Quantitative study of scars in the boundary section of the stadium billiard

Fernando P. Simonotti, Eduardo Vergini, and Marcos Saraceno
Departamento de Física, Comisión Nacional de Energía Atómica, Av. Libertador 8250, 1429 Buenos Aires, Argentina
(Received 11 April 1997; revised manuscript received 5 June 1997)

We construct a semiclassically invariant function on the boundary of the billiard, taken as the Poincaré section in Birkhoff coordinates, based on periodic orbit information, as an ansatz for the normal derivative of the eigenfunction. Defining an appropriate scalar product on the section, we can compute the *scar intensity* of a given periodic orbit on an eigenstate, as the overlap between the constructed function and the normal derivative on the section of the eigenstate. In this way, we are able to investigate how periodic orbits scar the spectrum and how a given eigenstate decomposes into *scar functions*. We use this scheme on the Bunimovich stadium. [S1063-651X(97)11509-4]

PACS number(s): 05.45.+b, 03.65.Sq, 03.40.Kf

I. INTRODUCTION

Since the observation of imprints of periodic orbits in quantum eigenfunctions, *scars*, by McDonald and Kaufmann [1], a vast amount of work has been done toward the understanding of this phenomenon. The numerical work and theoretical analysis of Heller [2] has been of great importance. Bogomolny [3] pushed the theory of scars further, his developments relied on the smearing of the probability density over a small energy range. A similar approach, but in phase space rather than in coordinate space, was used by Berry [4]. A theory for individual eigenstates was developed by Agam and Fishman [5], who constructed a semiclassical Wigner function. The integration of this Wigner function in a narrow tube along a periodic orbit gave them the scar weight. Smilansky [6] used the scattering approach to define a function on the Poincaré section, which was tested for scars. An important tool in the following analysis, the stellar representation, was developed by Tualle and Voros [7].

In this paper, we construct a semiclassically invariant function on the Poincaré section, built on a given periodic orbit, which we call the *scar function*, which can be extended to the domain via the Green theorem (5). We define the *scar intensity* as the overlap between this scar function and the corresponding reduction of the eigenfunction on the section, with a given measure, so as to mimic the overlap in the domain. Using this construction on the stadium billiard, we are able, by means of symbolic dynamics, to identify scars of single periodic orbits and of families of them in the quantum spectrum. Also, as we do not resort to energy smearing, we can decompose an eigenstate in periodic orbit functions (the scar functions).

This paper is organized as follows. In Sec. II we formulate our approach to the calculation of a scar measure, and introduce the necessary objects. In Sec. III we compute scars for the Bunimovich stadium, and analyze how different families of periodic orbits scar the corresponding eigenfunctions, particularly the whispering gallery and bouncing ball families. Our conclusions and closing remarks can be found in Sec. IV.

II. SCAR FUNCTION ON THE BOUNDARY

All the information of a given eigenfunction of the billiard (with Dirichlet boundary conditions) is contained in its normal derivative evaluated on the boundary. By means of the Green function we can obtain the wave function $\Psi_\nu(\mathbf{r})$, with wave number k_ν, in the domain in terms of its normal derivative:

$$\Psi_\nu(\mathbf{r}) = -\oint ds\; G_0(k_\nu;\mathbf{r},\mathbf{r}'(s))\,\frac{\partial \Psi_\nu}{\partial \mathbf{n}}(\mathbf{r}'(s)), \qquad (1)$$

where $G_0(k_\nu;\mathbf{r},\mathbf{r}'(s)) = (-i/4)H_0^{(1)}(k_\nu|\mathbf{r}-\mathbf{r}'(s)|)$ is the free Green function [9]. $H_0^{(1)}$ is the Hankel function of the first kind.

We thus treat the normal derivative as the fundamental irreducible object that will be tested for the presence of scars. The function

$$\phi_\nu(s) = \frac{\partial \Psi_\nu}{\partial \mathbf{n}}(\mathbf{r}'(s)) \qquad (2)$$

can be thought of as the coordinate representation of an abstract vector $|\phi_\nu\rangle$ in the Hilbert space of periodic square integrable functions on the boundary. This boundary is also the standard Poincaré section for the classical dynamics and reduces the motion to a canonical mapping in the Birkhoff coordinates (q,p) [10]. The coordinate q is related to the arc length coordinate at the boundary where the bounce takes place by $q = (s/\text{ perimeter})_{\text{mod}1}$; and $p = \vec{\mathbf{p}}\cdot\hat{\mathbf{t}}/|\vec{\mathbf{p}}|$ is the fraction of tangential momentum at this point.

The Fourier transform of Eq. (2) would represent it in the momentum representation, and a coherent state one would display its features in the Birkhoff coordinate plane. We follow [7] to choose this route. Other representations are, of course, possible, and have been used in this context. Smilansky [6], for example, used angle and angular momentum variables as phase-space coordinates, which is the natural description when employing scattering methods. However, on this basis the representation of diffraction effects on functions on the boundary is singular and difficult to observe. The Birkhoff coordinates, besides embodying the natural geometry of the billiard, avoid this problem by prescribing definite periodic functions as candidates for boundary eigenfunctions.

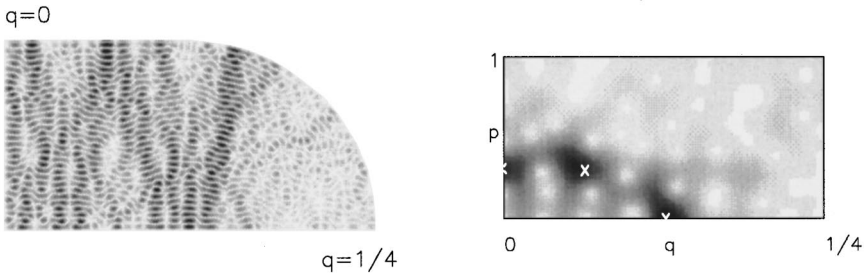

FIG. 1. Eigenfunction (left panel) and Husimi representation (right panel) for $k=100.954\,920\,427\,642$. This function is scarred by the periodic orbit with code 23202120. The crosses are the periodic points of this orbit.

As shown in Ref. [11], for eigenfunctions normalized to unity in the domain, in a neighborhood of a given k value, we have the quasiorthogonality relation for the normal derivatives,

$$\frac{1}{2k_\nu^2}\oint ds\ \hat{\mathbf{n}}\cdot\mathbf{r}\ \phi_\nu^*(s)\phi_\mu(s)=\delta_{\mu\nu}+\frac{(k_\mu-k_\nu)}{(k_\mu+k_\nu)}O(1). \quad (3)$$

Thus, with this measure, the set of eigenfunctions in a narrow range of k is orthonormal, and span a linear space of dimension $O(k)$.

It is then convenient, as we want to work exclusively on the boundary, to adopt a definition of scalar product

$$\langle\langle\phi|\psi\rangle\rangle\equiv\frac{1}{2k^2}\oint ds\ \hat{\mathbf{n}}\cdot\mathbf{r}\ \phi^*(s)\psi(s). \quad (4)$$

Any of these functions can be extended to the domain by means of Green's theorem; using it as an ansatz for the normal derivative, $\partial\Psi/\partial\mathbf{n}(s)$, and setting $\Psi(s)$ to zero,

$$\Psi_k(\mathbf{r})=\oint ds\left[\Psi(\mathbf{r}'(s))\frac{\partial G_0}{\partial\mathbf{n}}(k;\mathbf{r},\mathbf{r}'(s))-G_0(k;\mathbf{r},\mathbf{r}'(s))\frac{\partial\Psi}{\partial\mathbf{n}}(\mathbf{r}'(s))\right]. \quad (5)$$

Of course, Eq. (5) is not an eigensolution, because the limiting value of $\Psi(\mathbf{r})$, as $\mathbf{r}$ goes to the boundary, is not zero; that is to say, the function is discontinuous at the boundary. This function depends on the continuous parameter k, which controls the semiclassical limit.

With this definition, the normal derivatives $\phi_\nu(s)$ of eigenfunctions normalized *in the domain* are orthonormal (to order $1/k$) in a small range $\Delta k=(2\times$ perimeter/area).

For the phase space representation we construct coherent states with the correct space periodicity [7], defined as

$$\langle s|pq\rangle=\left(\frac{k}{\sigma\pi}\right)^{1/4}\sum_{a=-\infty}^{\infty}\exp[ikp(s-q-a)]\times\exp\left(-\frac{k}{2\sigma}(s-q-a)^2\right). \quad (6)$$

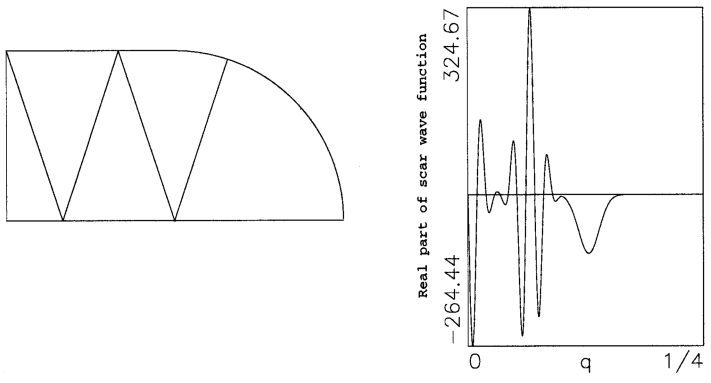

FIG. 2. Different representations of the scar function of a periodic orbit. Upper left panel: periodic orbit in the fundamental domain (symbolic code 23202120, following [14]). Upper right panel: real part of the scar wave function in the boundary. Lower left panel: probability density in the domain (via Green function). Lower right panel: Husimi representation.

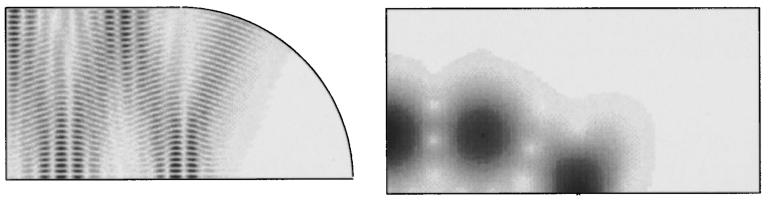

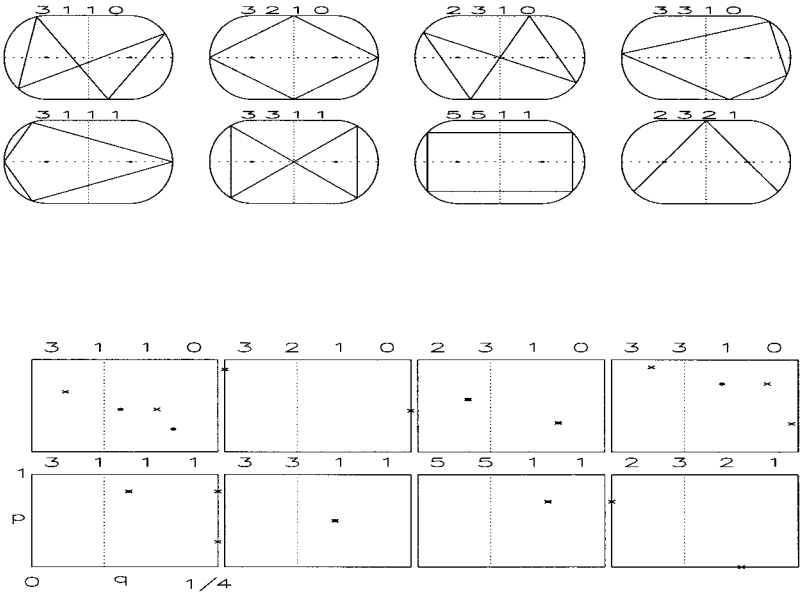

FIG. 3. Periodic orbits of four bounces in configuration space (upper panel) and in phase space (lower panel). In the latter plot, the points are depicted by dots or crosses, depending on the sign of p. The dotted vertical line is placed at the value of q where the discontinuity in curvature occurs.

This is a boundary wave packet, periodic in s, which is localized at the point (p,q) in the Birkhoff Poincaré section phase space.

A single wave packet represents a bounce off a specified point on the boundary with a given tangential momentum. Thus, to extract the phase-space contents of a given eigenfunction, we can construct the overlap

$$\mathcal{A}_\nu(p,q)=\frac{1}{|\langle\langle pq|pq\rangle\rangle|^{1/2}}\oint ds\ \langle pq|s\rangle\phi_\nu(s)\ \frac{\hat{\mathbf{n}}\cdot\vec{\mathbf{r}}}{2k_\nu^2}. \quad (7)$$

Thus a first visual display of the eventual localization and scarring of the eigenstates comes through the Husimi function

$$\mathcal{H}_\nu(p,q)=|\mathcal{A}_\nu(p,q)|^2. \quad (8)$$

We show an example of this for the stadium eigenfunction with $k=100.954\,920\,427\,642$ in Fig. 1.

Clearly, a first quantitative measure of the scarring of a periodic orbit would be

$$S'(\nu,\gamma)=\frac{1}{N}\sum_{i=1}^{N}\mathcal{H}_\nu(p_{\gamma_i},q_{\gamma_i}), \quad (9)$$

which averages the probability over the N points γ_i of the periodic trajectory γ. This measure was used by Muller and Wintgen in the context of the diamagnetic Kepler problem [8].

This average over the probabilities of the periodic points does not take into account the phase relations, due to semiclassical propagation, between them. Therefore, it seems a more convenient strategy to average the *amplitudes* with the proper phase differences. A better measure, then, is provided by the construction of the scar function

$$\langle s|\varphi(k,\gamma)\rangle=\frac{1}{|\langle\langle\varphi(k,\gamma)|\varphi(k,\gamma)\rangle\rangle|^{1/2}}\sum_{j=1}^{N}\exp(if_j)\langle s|p_jq_j\rangle, \quad (10)$$

where q_i and p_i are the Birkhoff coordinates of the periodic points.

The phases f_j are defined by

$$f_j=kl_j-j\pi-\frac{\pi}{2}\nu_j, \quad (11)$$

where l_j is the distance in configuration space between the initial point of the periodic orbit and the jth point. The second term takes into account the boundary conditions (Dirichlet), and the third the conjugate points along the trajectory. The inclusion of these phases is very important in the determination of the existence of scars.

The total accumulated phase f_N will not, in general, be a multiple of 2π. In order to have an invariant function, depending only on the orbit and not on the starting point, we add an additional phase to each point, so as to make $f_N=2\pi n$, with n an integer:

$$f_j\rightarrow f_j+\frac{j}{N}\alpha, \quad (12)$$

with α the minimum beetween $(f_N)_{\mod 2\pi}$ and $2\pi-(f_N)_{\mod 2\pi}$. This state is a coherent sum over a periodic orbit and, thus, is a good candidate for an invariant probe depending only on the orbit.

A. Scar intensity $S_\gamma(k_\nu)$ and scar length spectrum $\tilde{S}_\gamma(l)$

We define the scar intensity

$$S(\nu,\gamma)=|\langle\langle\varphi(k_\nu,\gamma)|\phi_\nu\rangle\rangle|^2. \quad (13)$$

Notice that k is set to k_ν in $\langle\varphi(k,\gamma)|$. This measure of the scar intensity differs from Eq. (9) mainly by interference terms.

Each wave packet in Eq. (10) represents a localized plane wave hitting the boundary at a specified point in a specified direction. Thus Eq. (10), when seen in this light, can be assimilated to a superposition of plane waves which privileges the wave directions associated with the periodic orbit.

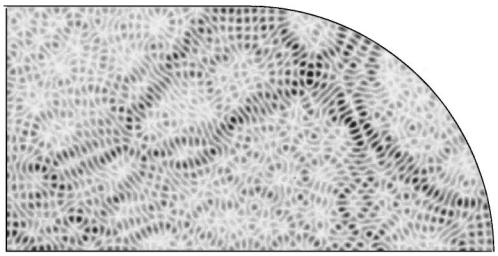

FIG. 4. Odd-odd stadium eigenfunction with $k=130.4886\ 755\ 073$.

For example, in Fig. 2 we show a periodic orbit of the stadium billiard and the associated scar wave function in different representations, with $k=100.954\ 920\ 427\ 642$ (the same as in Fig. 1).

The scar wave function in the domain is a solution of the Helmholtz equation with a given value of k. So, if we expand it in terms of the exact eigenfunctions, we expect that the more significant contributions come from the eigenfunctions with closer k_ν to k [more precisely, $|k-k_\nu|\leqslant(2\times$ perimeter/area)]. Then, using the quasiorthogonality relation (3), the norm of the scar wave function in the domain is 1 to order k^{-1}. Our aim is to describe this subspace in terms of states constructed on periodic orbits, as in Eq. (13). This is not dissimilar to the task of describing them in terms of plane or cylindrical waves. However, the peculiar linear combinations taken in Eq. (10), being semiclassically invariant under the bounce map, should provide the most important correlations.

The density of states of the billiard has a semiclassical representation [12] as

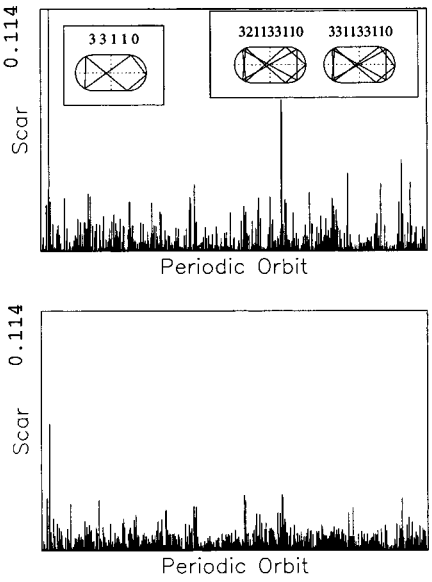

FIG. 5. S and S' functions for k=130.488 675 507 3 (upper and lower panel, respectively.) In the leftmost inset we see the periodic orbit with maximum scar intensity; in the rightmost one, the orbits that give the two secondary peaks. The orbits are ordered by increasing number of bounces, up to nine.

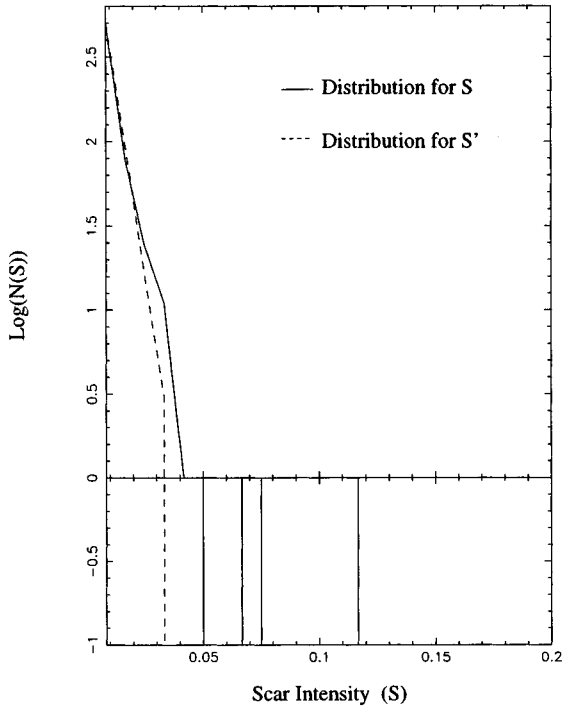

FIG. 6. Distribution of scar intensities, $N(S)$, for S (full line) and S' (dashed line) for $k=130.488\ 675\ 507\ 3$. The base of the logarithm is 10.

$$d_{scl}(k)\approx\langle d(k)\rangle+\frac{1}{\pi}\sum_p\sum_{r=1}^{\infty}\frac{l_p}{|\det(\mathbf{I}-\mathbf{T}_p^r)|^{(1/2)}}\times\cos[r(kl_p-\nu_p\pi/2)], \tag{14}$$

where the first sum is done over primitive periodic orbits, the second sum takes into account their repetitions, l_p is the

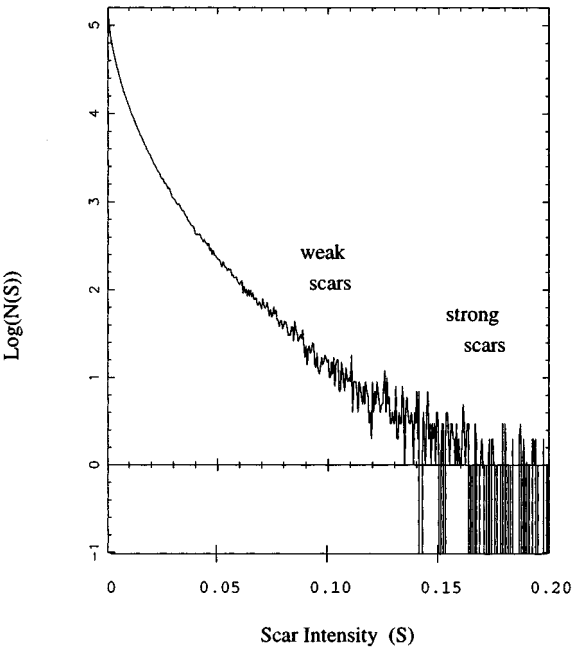

FIG. 7. Distribution of scar intensities, $N(S)$, for the 1654 consecutive eigenfunctions and first 617 periodic orbits. The base of the logarithm is 10.

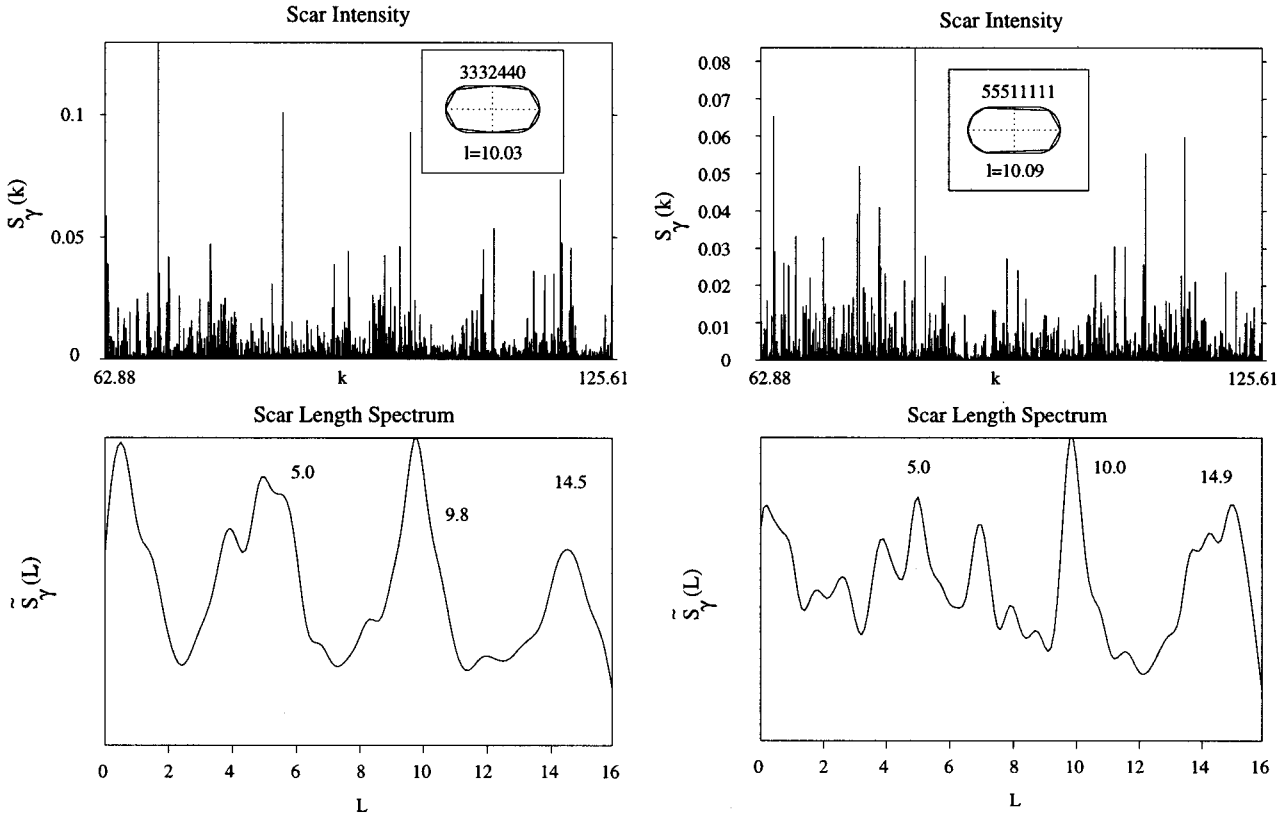

FIG. 8. Scar intensity and scar length spectrum for some whispering gallery periodic orbits. Upper left panel: scar intensity for periodic orbit 3332440. Lower left panel: scar length spectrum for periodic orbit 3332440. Upper right panel: scar intensity for periodic orbit 55511111. Lower right panel: scar length spectrum for periodic orbit 55511111.

length of the orbit, ν_p is the Maslov index, and $\mathbf{T}_p$ is the monodromy matrix. The smooth part of the density of states is given by $\langle d(k)\rangle$. The Fourier transform of Eq. (14) provides a distribution linked more directely to the classical motion, i.e., the *length spectrum*, which shows well-defined peaks at the lengths (actions) of periodic orbits.

In order to focus more specifically on the scarring features of a single orbit along the spectrum, we set γ to a given periodic orbit in Eq. (13),

$$S_\gamma(k_\nu)=|\langle\langle\varphi_\gamma(k_\nu)|\phi_\nu\rangle\rangle|^2. \tag{15}$$

Its Fourier transform is

$$\tilde{S}_\gamma(l)=\sum_{k_\nu} S_\gamma(k_\nu)\exp(ik_\nu l), \tag{16}$$

which we will call the scar length spectrum.

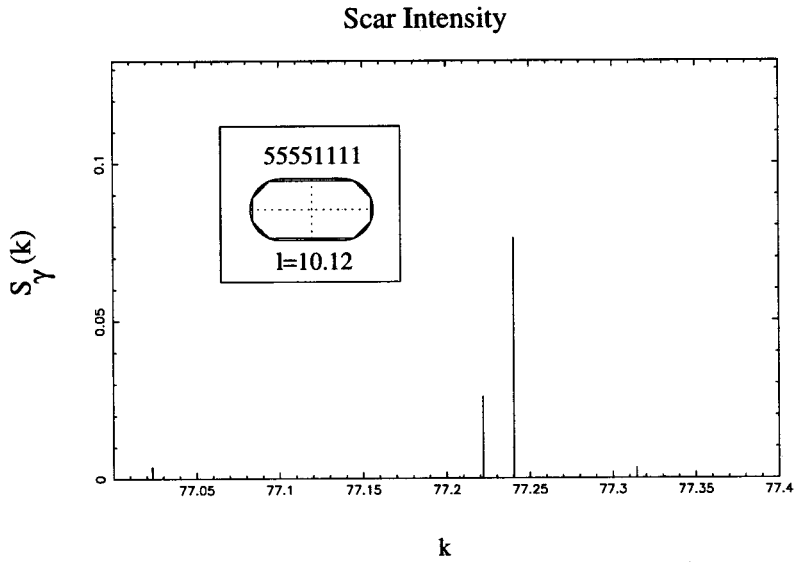

FIG. 9. Scar intensity for a range of k, for the periodic orbit depicted in the inset.

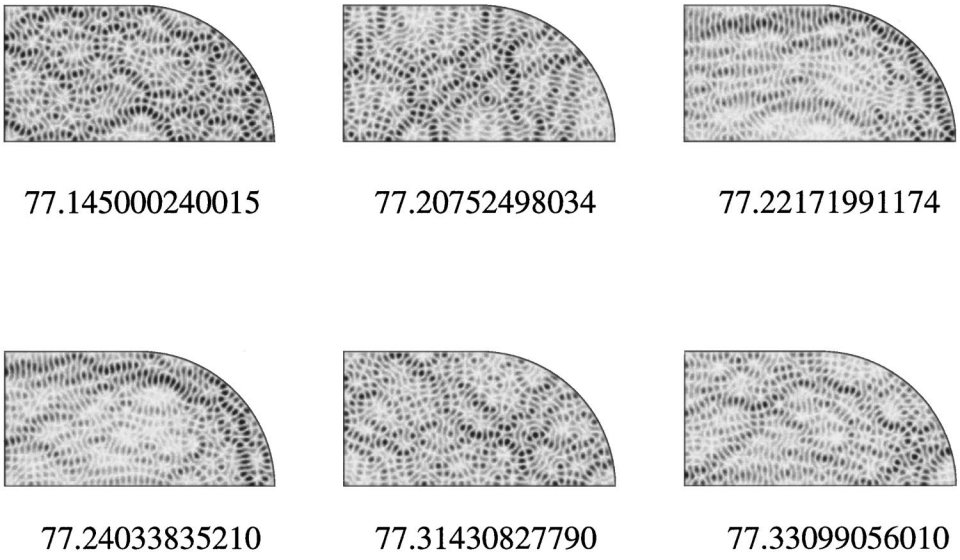

FIG. 10. Group of eigenfunctions in the same range of k of Fig. 9.

If periodic orbits obeyed Bohr-Sommerfeld-like quantization conditions, we would expect a periodic behavior of $S_\gamma(k_\nu)$ with a period $\Delta k=\pi/L_\gamma$. This implies periodic sequences of scarred states along the spectrum . These states have been also observed in other billiards [5,6]. Here we test for these periodicities directly in the scar length spectrum. The periodicities would be exact but for the fact that the periodic orbit basis is not orthonormal, and the quantization rule of a single orbit does not lead necessarily to a quantized state.

To eliminate spurious behavior of the Fourier transform due to end effects of the k interval, we multiply the scar intensity in Eq. (16) by a function vanishing at the ends; typically a quadratic function [13]. The scar length spectrum still shows large fluctuations with very clear local average peaks at certain lengths. This local structure is evidenced by averaging the resulting Fourier transform.

III. BUNIMOVICH STADIUM

The boundary of the stadium billiard is defined by two semicircumferences connected by two straight segments. Of all the possible stadia, we consider only the one with relation 2:1 beetween its total length and height, and we will scale the lengths in such a way that the perimeter is $4+2\pi$ and the area is $4+\pi$.

At the classical level, we will describe the periodic orbits following Biham and Kvale [14]. Their symbolic dynamics is a six-symbol one where each symbol corresponds to a bounce off the boundary: (i) 0: A bounce off the lower straight segment. (ii) 1: A clockwise bounce off the left

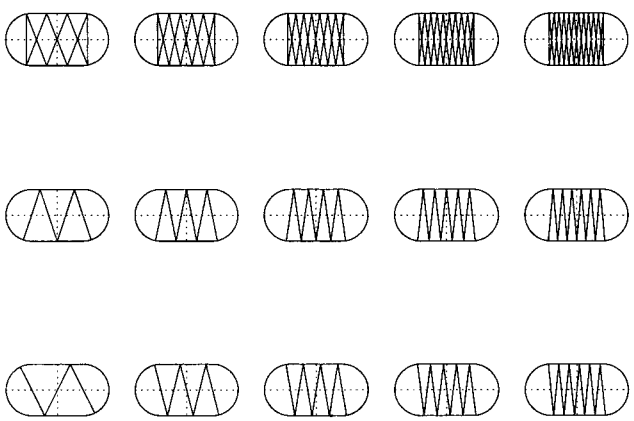

FIG. 11. Bouncing ball periodic orbits, first five members of families A, B, and C (first, second, and third rows, repectively).

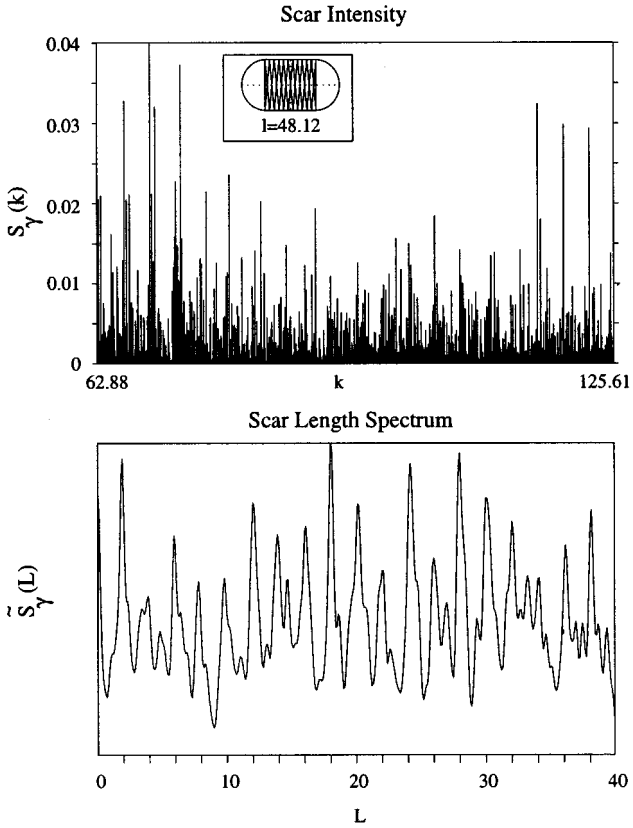

FIG. 12. Scar intensity and scar length spectrum for a periodic orbit in the bouncing ball limit.

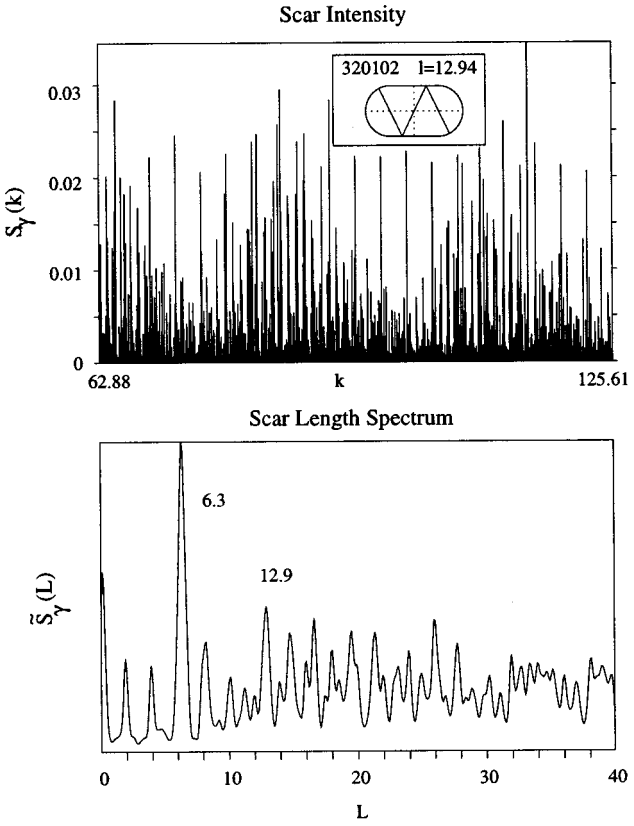

FIG. 13. Scar intensity and scar length spectrum for a periodic orbit not in the bouncing ball limit.

semicircle or a single anticlockwise bounce off the left semicircle. (iii) 2: A bounce off the upper straight segment. (iv) 3: An anticlockwise bounce off the right semicircle or a single clockwise bounce off the left semicircle. (v) 4: A not single anticlockwise bounce off the left semicircle. (vi) 5: A not single clockwise bounce off the right semicircle. A bounce is a single one if it is not preceded or followed by a bounce off the same section of the boundary.

This dynamics has to be pruned. This pruning is geometrical and corresponds to the symbolic dynamics of the stadium of infinite length. As the length is made finite, more pruning rules appear (of a dynamical character), as described in Ref. [15].

Using this symbolic description we have computed all the periodic orbits up to ten bounces and a few selected ones of much higher periods, and we have ordered them (somewhat arbitrarily) by their number of bounces and symbolic codes. In Fig. 3 we show the correspondence of these calculated orbits as projections in configuration space and in the Birkhoff Poincaré (desymmetrized) section.

At the quantum level, we compute the energy levels and eigenfunctions by the scaling method [11], which gives directly all eigenvalues and eigenfunctions very precisely and efficiently. We have computed 1654 consecutive levels and their eigenfunctions ranging from $k \approx 62.8$ and $k \approx 125.2$; and other selected ones.

A. Periodic orbit decomposition of eigenfunctions

In Fig. 5 we demostrate the advantage of using the present scar function as opposed to the simple unphased average, S', of Eq. (9). We take one of the scarred wave functions of Heller [2] (Fig. 4) and plot the quantities S and S' as a function of the periodic orbit label γ (Fig. 5). The periodic orbits are ordered in increasing periods and, within each period, by symbolic codes. Recurrences in S sometimes occur due to the existence of orbits of period $n \times p$ that almost retrace n times the periodic orbit of period p. However, many recurrences are also due to short homoclinic and heteroclinic excursions.

The peaks are more clearly defined in the S plot, due to the enhancement brought about by the semiclassical dynamics f_j (note that the maximum scar value is around 0.114 for S and 0.06 for S'). Due to the binning of the interval, the strongest peak of S' overlaps with one of the secondary peaks of S. In the leftmost inset in Fig. 5 we show the periodic orbit that scars this eigenfunction the most. Moreover, the two most prominent secondary peaks come from two different homoclinic excursions of this orbit (see the rightmost inset in Fig. 5).

Both measures indicate the presence of scars, i.e., amplitudes larger than the average fluctuation. However, as S captures the phase relations of periodic orbits, the basis $|\varphi(k,\gamma)\rangle$ is ''closer'' to reflecting the invariant properties characteristic of the stadium. Thus we expect the amplitudes S to have much larger fluctuations (and, therefore, clearer scars) than S'. This fact is shown clearly in Fig. 6, where we show the distribution of scar intensities, $N(S)$. The small amplitudes are distributed approximately as an exponential. The distribution corresponding to S is much broader than that of S'. For this strongly scarred state, there is a large region beetween 0.07 and 0.114 where no scar intensities appear. So, $\log_{10}(N(S))$ goes to $-\infty$ in this region. At 0.114 a single periodic orbit gives a large scar, yielding $\log_{10}(N(S))=0$. The occurrence of this peak is, however, a rare event. The secondary peaks, due to homoclinic excursions of the periodic orbit which gives the strongest peak, are to be found at, approximately, $S=0.071$ and 0.066.

We have tested all 1654 eigenfunctions in the range beetween $k \approx 62.8$ and $k \approx 125.2$ against scarring by the first 617 periodic orbits (i.e., up to nine bounces), giving a total of approximately 1 000 000 scar intensities. The distribution of these intensities is shown in Fig. 7. We can observe three different sections: strong scars, weak scars, and the region closer to $S=0$, where most of the scar intensities are (there are around 1 000 000 scar intensities from $S=0$ to 0.1, whereas only 760 are to be found with $S>0.1$.) This distribution is very different from the Porter-Thomas result. The reason is that the basis of $\langle s|\varphi(k,\gamma)\rangle$ is not orthonormal and, moreover, is chosen so as to be closely related to the dynamics. Should we examine the scars on any other basis, unrelated to the dynamics of the stadium, for example a plane-wave basis, we would only expect a statistical distribution of the intensities, in accordance to random matrix theories.

The presence of the peaks in the strong scar region in Fig. 7 quantifies the scar phenomenon and shows, in accordance with Shnirelman's theorem [16], that scarring is exceptional. However, it is the only remaining signature of the specific classical behavior of the system, as embodied in its periodic orbits.

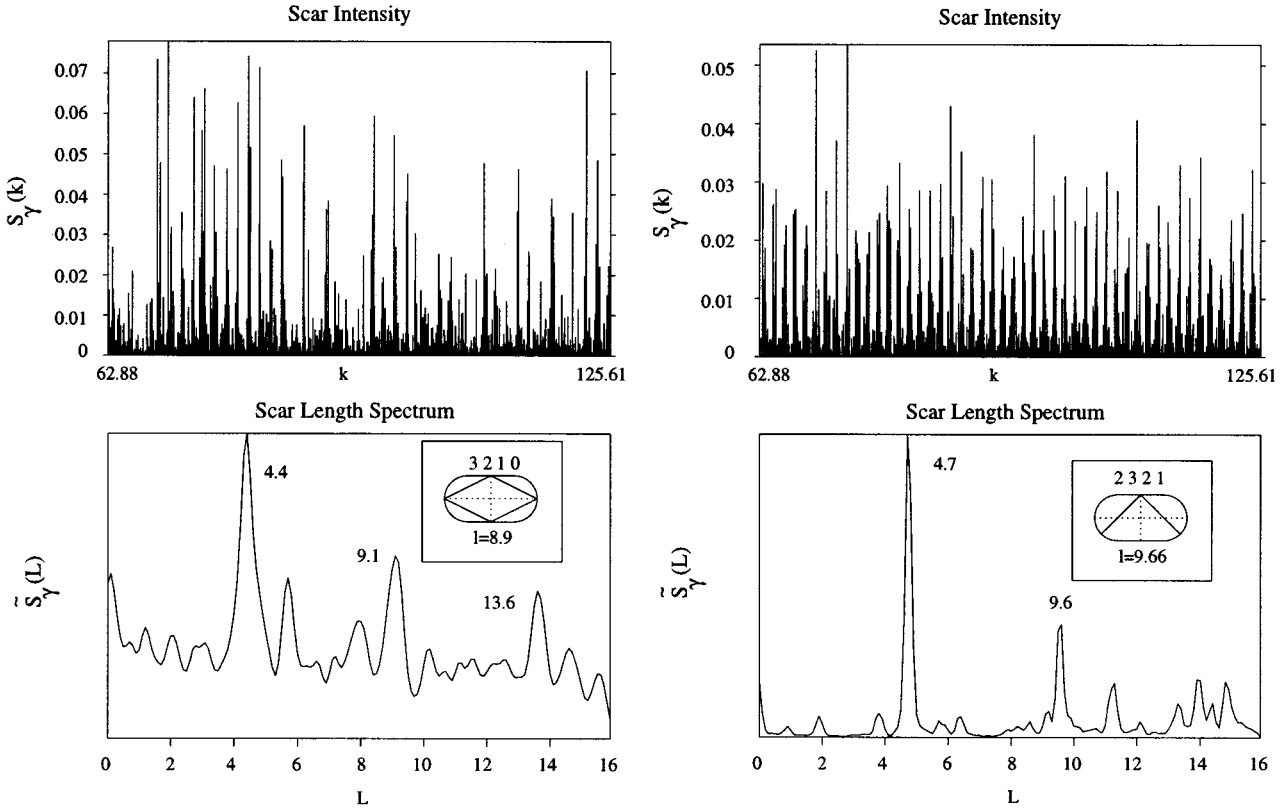

FIG. 14. Scar intensity and scar length spectrum for some low period periodic orbits. Left panels: scar intensity and scar length spectrum for periodic orbit 3210. Right panels: scar intensity and scar length spectrum for periodic orbit 2321.

B. Families of periodic orbits

1. Whispering gallery family

This family is composed by trajectories of code $5^n0^a1^m2^b$; where a and b are 0 or 1, and m and n are positive integers (as there is time-reversal symmetry, the same orbit can be described by the code $3^n2^b4^m0^a$). The whispering gallery limit is approached as $m,n\rightarrow\infty$ simultaneously. For the periodic orbit to exist, as this limit is approached, the difference between m and n should remain finite; the largeness of this difference being determined by the length of the stadium. This is a clear example of dynamical pruning (as opposed to geometrical pruning, i.e. independent of the length of the stadium).

We have found that the whispering gallery trajectories that show a more pronounced periodicity in the scarring are those defined by $m>2$ and $n>2$, independent of their symmetry or value of a and b. Of course, where high symmetry is present, the periodicity is stronger.

We show in Fig. 8 the function $S_\gamma(k)$ and the scar length spectrum for some whispering gallery periodic orbits. We see how the scar length spectrum shows clearly the periodicity of $S_\gamma(k)$, defined by the fundamental length of the orbit and its repetitions. (The lengths shown are multiples of $L_\gamma/2$ because of the symmetry of the orbit.)

The width of the group of states that participate in the scarring is constant in the region considered. This means that more and more states are involved in one ''Bohr-Sommerfeld'' interval. However, only a few, typically one or two, show visible scars. In Fig. 8 (first panel), where the width of the groups is approximately $\Delta k\approx 1.27$, the first group involves around 35 states at $k\approx 62.88$ and the last involves 45 at $k\approx 125.60$ in accord with the change in the density of states.

We can exemplify how well the scar intensity picks up the scarred eigenstates. We look for scars in the region delimited by $k\approx 77.14$ and $k\approx 77.34$ for the periodic orbit with code 55551111 (see Fig. 9). We find two contiguous states that are scarred by this periodic orbit, namely, $k=77.221\ 719\ 911\ 74$ and $k=77.240\ 338\ 352\ 10$. The probability densities of these eigenfunctions confirm this fact: see Fig. 10. Notice the similarity between both eigenfunctions and between them and the mentioned whispering gallery periodic orbit.

2. Bouncing ball family

This family is composed of three subfamilies, following Ref. [17], whose symbolic codes are $33(02)^n11(02)^n$ (family A), $23(20)^n21(20)^n$ (family B), and $3(20)^n1(02)^n$ (family C). The bouncing ball limit is $n\rightarrow\infty$, where the resulting periodic orbit has increasingly smaller x component of the wave number k. We will consider the first five members of each family, with periods ranging from 6 to 24 (see Fig. 11).

The bouncing ball eigenstates are approximately described by those of a rectangle with the same size as the one inscribed in the stadium. So the quantized wave numbers are given by $k\approx\pi\sqrt{n_x^2+n_y^2}$, where $n_{x(y)}$ is the number of nodes along the $x(y)$ axis.

The preceding considerations tell us not to expect a scar length spectrum that is peaked in the length of the given periodic orbit and its multiples. This is so because there is no such periodicity in the scar intensities for the bouncing ball

families. This is what we observe for those orbits tending to the bouncing ball limit; see an example in Fig. 12. Notice, though, how for large L the peaks appear for even L. This fact is related to the multiple bounces between the two straight segments of the billiard, approximately of length 2. Some of the first few orbits of each family show a single peak in the length of the orbit, with no peaks (or small ones) in the multiples; see an example in Fig. 13.

3. Other periodic orbits

As ''scars are scarce'' [6], the scar length spectrum for most periodic orbits shows no peaks in the associated length. Other orbits show rather more complex patterns with many lengths that are not easily assigned to other periodic orbits (whether in the homoclinic family of the first or not). However, there is a small set of orbits for which the scar intensities have the expected periodicity (some examples in Fig. 14).

IV. CONCLUSIONS

We have constructed a quantitative measure for the presence of scars that, by taking into account semiclassical phase correlations, provides a sharper indication of their presence. The measure is constructed as an ansatz for the normal derivative of a state representing a pure stationary scar and therefore testing the most the irreducible contents of the eigenfunctions as contained in the normal derivative. Thus it is very suitable for numerical calculations, as it involves only boundary integrations, avoiding completely— except for graphical display— any integration over the domain of the billiard.

We have provided examples of the decomposition of a single eigenstate into scar functions and of the systematic way in which some orbits appear in the k spectrum. The scar intensities show how an eigenstate is distributed on the basis of quantum states constructed from periodic orbits. Such a basis is clearly not orthogonal (and, probably, overcomplete). The investigation of the properties of this basis remains to be done.

By testing many orbits and many eigenstates, we have found that scars are quite rare, in accordance to expectations from Shnirelman's theorem [16]. Even less frequent is to find sequences of states scarred periodically (in k) by a given orbit. Most eigenfunctions decompose in periodic orbits in such a way that no one prevails over the others. This, in turn, implies no clear scars in most instances. The families that show stronger scars are the whispering gallery and the bouncing ball ones, both being rather exceptional families.

ACKNOWLEDGMENTS

This work was partially supported by CONICET PIA 6950 and by the EC Program/ARG/B7-3011/94/27.

[1] S. W. McDonald, Ph.D. thesis, Lawrence Berkeley Laboratory LBL 14837 (1983).
[2] E. J. Heller, in *Chaos and Quantum Physics*, Proceedings from Les Houches 1989 (North-Holland, Amsterdam, 1989).
[3] E. B. Bogomolny, Physica D **31**, 169 (1988).
[4] M. V. Berry, Proc. R. Soc. London, Ser. A **423**, 219 (1989).
[5] O. Agam and S. Fishman, Phys. Rev. Lett. **73**, 806 (1994).
[6] D. Klakow and U. Smilansky, J. Phys. A **29**, 3213 (1996).
[7] J. M. Tualle and A. Voros, Chaos Solitons Fractals **5**, 1085 (1995).
[8] K. Muller and D. Wintgen, J. Phys. B **13**, 2693 (1994).
[9] M. Berry and M. Wilkinson, Proc. R. Soc. London, Ser. A **392**, 15 (1984).
[10] V. I. Arnold and A. Avez, *Ergodic Problems of Classical Mechanics* (Addison-Wesley, Reading, MA, 1989).
[11] E. Vergini and M. Saraceno, Phys. Rev. E **52**, 2204 (1995).
[12] U. Smilansky, in *Mesoscopic Quantum Physics*, Proceedings from Les Houches 1994 (North-Holland, Amsterdam, 1995).
[13] T. Prosen (unpublished).
[14] O. Biham and M. Kvale, Phys. Rev. A **46**, 6334 (1992).
[15] K. T. Hansen and P. Cvitanovic (unpublished).
[16] A. Shnirelman, Usp. Mat. Nauk. **29**, 181 (1974).
[17] G. Tanner, J. Phys. A **30**, 2863 (1997).